Magnetic ordering in the static intermediate-valent cerium compound Ce_2RuZn_4

Volker Eyert*
Center for Electronic Correlations and Magnetism, Institut für Physik, Universität Augsburg, D-86135 Augsburg, Germany

Ernst-Wilhelm Scheidt and Wolfgang Scherer
Chemische Physik und Materialwissenschaften, Institut für Physik, Universität Augsburg, D-86135 Augsburg, Germany

Wilfried Hermes and Rainer Pöttgen
Institut für Anorganische und Analytische Chemie, Westfälische Wilhelms-Universität Münster, D-48149 Münster, Germany

(Received 21 August 2008; revised manuscript received 20 November 2008; published 15 December 2008)

The low-temperature behavior of Ce_2RuZn_4 has been investigated. Specific-heat and magnetic-susceptibility data reveal an antiferromagnetic transition at a Néel temperature of 2 K. Ce_2RuZn_4 is a static intermediate-valent compound with two crystallographically independent cerium atoms. The magnetic data clearly show that only one cerium site is magnetic (Ce^{3+}), while the second one carries no magnetic moment. The experimental data are interpreted with the help of first-principles electronic structure calculations using density-functional theory and the augmented spherical wave method. The calculations reveal the occurrence of two different cerium sites, which are characterized by strongly localized magnetic moments and strong Ce-Ru bonding.

DOI: 10.1103/PhysRevB.78.214420 PACS number(s): 71.20.Eh, 75.50.Cc, 75.30.Sg

I. INTRODUCTION

Ternary intermetallic compounds in the system Ce-Ru-*X*, where *X* is an element of the third, fourth, or fifth main group, have been intensively studied in recent years. This is due to the fact that these materials exhibit peculiar structural and physical properties, where the transition-metal ruthenium seems to play a key role. In comparison to related compounds with other transition metals, ruthenium often shows extremely short Ce-Ru distances, even much shorter than the sum of the covalent radii of 289 pm.[1] Already the binary Laves phase $CeRu_2$,[2] which is a superconductor below 6.2 K,[3] is extraordinary. In this compound, the cerium atoms are in an intermediate-valent state and the *a* lattice parameter is much smaller than that of $NdRu_2$. When it comes to the ternary compounds, these effects are even more pronounced. The recently reported indium compounds $CeRu_{0.88}In_2$, $Ce_{16}Ru_8In_{37}$, $Ce_3Ru_2In_2$, and $Ce_3Ru_2In_3$ exhibit extremely short Ce-Ru distances,[4–7] which are directly associated with a strong tendency of some of the cerium sites toward tetravalency.

The stannide CeRuSn also shows this peculiar behavior.[8,9] The room-temperature modification adopts a superstructure of the CeCoAl type and the two crystallographically independent cerium sites are ordered on distinct positions. In particular, the intermediate-valent Ce1 atoms have very short Ce1-Ru distances of only 233–246 pm. Consequently, our electronic structure calculations revealed strong Ce-Ru bonding.

Another example for trivalent/intermediate-valent cerium ordering is the structure of Ce_2RuZn_4.[10] This structure type crystallizes in the space group $P4/nmm$ with 2 f.u./cell and two twofold cerium sites with distinctly different coordination. Preliminary magnetic-susceptibility investigations underlined the idea of trivalent/intermediate-valent cerium ordering. Extending our systematic studies of such ruthenium-based intermetallic compounds we here report on a comprehensive investigation of the low-temperature properties of Ce_2RuZn_4. In particular, our work includes x-ray diffraction, specific heat, and magnetic-susceptibility measurements, as well as electronic structure calculations.

II. EXPERIMENTAL

A. Synthesis

Starting chemicals for the preparation of Ce_2RuZn_4 were a cerium ingot (Johnson Matthey, purity of >99.9%), ruthenium powder (Degussa-Hüls, approximately 200 mesh, purity of >99.9%), and zinc granules (Merck, purity of >99.9%). Pieces of the cerium ingot were first arc melted to a small button under argon.[11] The argon was purified before with molecular sieve, silica gel, and titanium sponge (900 K). The elements were then mixed in the 2:1:4 atomic ratio (ruthenium powder was cold pressed to a pellet of 6 mm diameter) and arc welded in a tantalum ampoule under an argon pressure of 700 mbar. The ampoule was subsequently placed in a water-cooled sample chamber of a high-frequency furnace (Hüttinger Elektronik, Freiburg, type TIG 5/300).[12] The heat treatment was similar to our previous experiments:[10] three times for 1 min at 1360 K, for 10 min at 1360 K, rapid cooling to 920 K, and a final annealing at that temperature for another 2 h followed by quenching.

B. Powder x-ray diffraction

The purity of the sample was checked through a Guinier powder pattern using Cu $K\alpha 1$ radiation and α quartz ($a=491.30$ pm, $c=540.46$ pm) as an internal standard. The tetragonal lattice parameters were obtained from a least-squares refinement of the Guinier powder data. The refined lattice parameters [$a=719.6(1)$ pm, $c=520.0(1)$ pm] are in good agreement with the previously reported data [$a=719.6(1)$ pm, $c=520.2(1)$ pm].[13] No impurity phases have been detected on the level of x-ray powder diffraction.

C. Specific heat and magnetic susceptibility

The temperature-dependent heat capacity was investigated by means of a quasiadiabatic step heating technique employing a Quantum Design Physical Properties Measurement System (PPMS). The measurements were performed on a polycrystalline sample thermally connected by grease (Apiezon-N) at temperatures ranging from 1.8 up to 300 K. For temperatures below 2 K, down to about 80 mK, specific-heat data were also collected in a ^{3}He/^{4}He-dilution-cryostat using a relaxation method.[14] The uncertainty of the measurements reported in this paper is estimated to be below 3%. The magnetic measurements in the temperature range $1.8\ \mathrm{K} < T < 300\ \mathrm{K}$ were done using a Quantum Design MPMS7 superconducting quantum interference device (SQUID) magnetometer.

III. THEORETICAL METHOD

The calculations are based on density-functional theory (DFT) and the local-density approximation (LDA). They were performed using the scalar-relativistic implementation of the augmented spherical wave (ASW) method (see Refs. 15 and 16, and references therein). In the ASW method, the wave function is expanded in atom-centered augmented spherical waves, which are Hankel functions and numerical solutions of Schrödinger's equation, respectively, outside and inside the so-called augmentation spheres. In order to optimize the basis set, additional augmented spherical waves were placed at carefully selected interstitial sites. The choice of these sites as well as the augmentation radii was automatically determined using the sphere-geometry optimization algorithm.[17] Self-consistency was achieved by a highly efficient algorithm for convergence acceleration.[18] The Brillouin-zone integrations were performed using the linear tetrahedron method with up to 105 **k** points within the irreducible wedge.[16,19]

In the present work, we used a full potential version of the ASW method, which was developed only very recently.[20] In this version, the electron density and related quantities are given by a spherical harmonics expansion inside the muffin-tin spheres. In the remaining interstitial region, a representation in terms of atom-centered Hankel functions is used.[21] However, in contrast to previous related implementations, we here get away without needing a so-called multiple-κ basis set, which fact allows for a very high computational speed of the resulting scheme.

IV. RESULTS AND DISCUSSION

A. Crystal chemistry

Ce_2RuZn_4 crystallizes with a peculiar structure type with space group $P4/nmm$.[10] Since the crystal chemistry of this zinc-rich intermetallic compound has been described in detail in our previous work,[10] here we focus only on the cerium coordination, which is responsible for the distinctly different magnetic behavior of the two cerium sites. A view of the Ce_2RuZn_4 structure approximately along the c axis is presented in Fig. 1. The zinc atoms build up a complex three-dimensional network, which leaves two different kinds of channels parallel to the c axis. They are filled by the cerium and ruthenium atoms. As emphasized in the right-hand part of Fig. 1, the trivalent Ce1 atoms have 12 nearest neighbors of only the zinc type. In contrast, the intermediate-valent (nearly tetravalent) Ce2 atoms have a smaller coordination number of ten atoms with two ruthenium and eight zinc sites. However, the most striking structural feature are the short Ce2-Ru distances of 260 pm, which are even shorter than the sum of the covalent radii of 289 pm.[1] This seems to be a characteristic of ruthenium and leads to a destabilization of the cerium valence. The peculiar electronic properties, which arise from this unusual crystal chemistry, are addressed below.

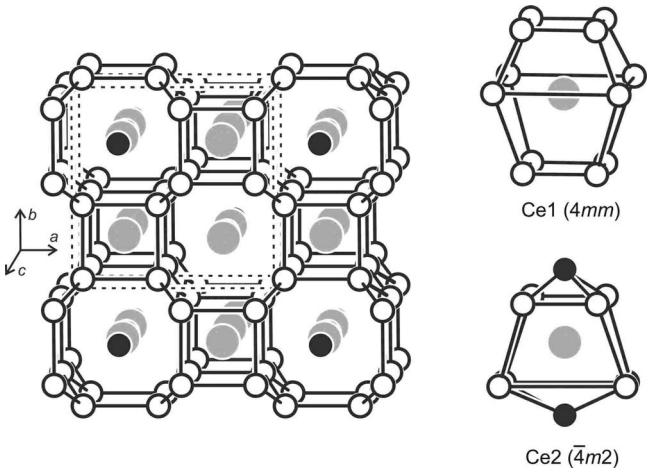

FIG. 1. The crystal structure of Ce_2RuZn_4: (left-hand side) view of the structure approximately along the c axis and (right-hand side) coordination polyhedra and site symmetries of the two crystallographically independent cerium sites. The cerium, ruthenium, and zinc atoms are drawn as medium gray, filled, and open circles, respectively.

B. Specific heat

In Fig. 2, the molar specific-heat capacity divided by temperature C/T of Ce_2RuZn_4 is displayed in a semilogarithmic plot for temperatures between 0.08 and 300 K. A clear peak at 2 K indicates a pronounced magnetic contribution to the heat capacity. In order to extract the magnetic contribution of the specific heat we determined the lattice contributions theoretically using a single Debye term and two Einstein modes. In this calculation, we fixed the number of internal degrees of freedom to 21, according to the seven atoms in the unit cell. Using a weight distribution of 1:2:4, we obtained a Debye temperature of $\Theta_D = 96$ K and two Einstein modes of $\Theta_{E1} = 129$ K and $\Theta_{E2} = 238$ K. The solid red line in Fig. 2 shows the corresponding result taking into account an electronic contribution of $\gamma = 30\ \mathrm{mJ/mol\ K^2}$. Below 1 K, the specific heat of Ce_2RuZn_4 increases slightly giving rise to a nuclear electronic Schottky contribution. We have calculated the hyperfine contributions to the heat capacity originating in zero magnetic field mainly from the quadruple moments of ^{101}Ru and ^{67}Zn leading to an average local internal electrical-field gradient of $V_{zz} = (5 \pm 0.8) \times 10^{22}\ \mathrm{V/m^2}$.

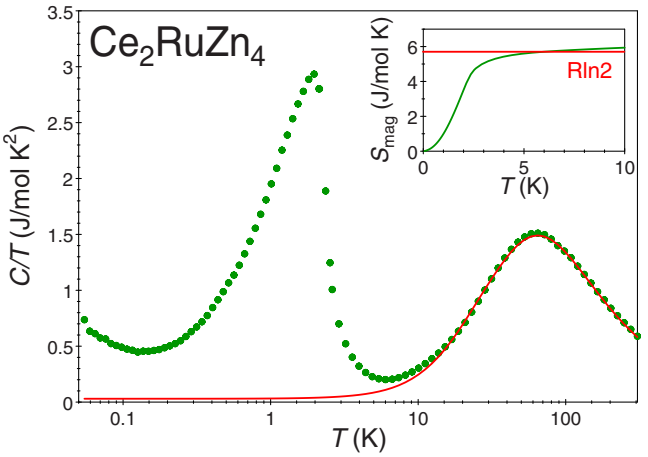

FIG. 2. (Color online) Specific heat divided by temperature vs log T of Ce_2RuZn_4 in the temperature range between 50 mK and 300 K. The slight increase in C/T below 1 K is mainly due to the nuclear quadrupole moments displayed by the ^{101}Ru and ^{67}Zn isotopes; the solid red line represents the lattice and electronic contributions. The inset shows the magnetic entropy. The red line displays $S_{mag}=R$ ln 2, which is the limit for a two level system.

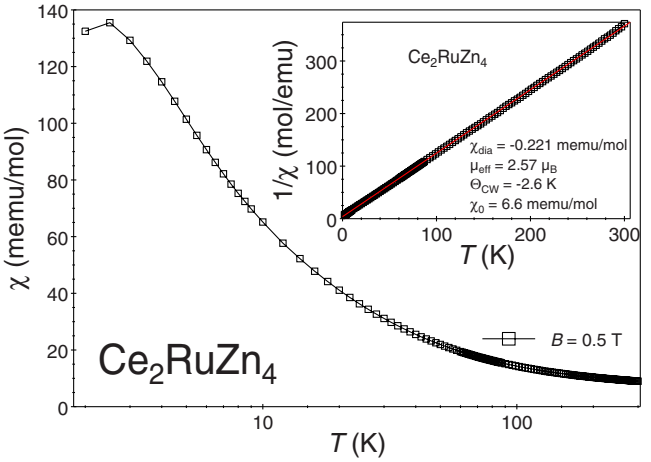

FIG. 3. (Color online) The magnetic susceptibility χ vs log T of Ce_2RuZn_4. At low temperature the beginning of an antiferromagnetic transition is observed. The inset exhibits the inverse susceptibility $1/\chi$ vs T. The solid line is a least-squares fit according to the modified Curie-Weiss law.

Subtracting the calculated electronic, lattice, and nuclear parts from the total specific-heat data results in the magnetic contribution of specific heat C_{mag}. Subsequent integration of C_{mag}/T leads to the magnetic entropy according to

$$S_{mag} = \int \frac{C_{mag}}{T} dT = R \ln(2S+1).$$

Here, S_{mag} and S refer to the magnetic entropy and the spin, respectively. The corresponding graph is shown in the inset of Fig. 2. The resulting magnetic entropy of R ln 2 is due to a two level $S=1/2$ state.

C. Magnetic susceptibility

The magnetic configuration of the Ce ion can be proven by susceptibility measurements $\chi(T)$. Our susceptibility data collected at a field of 0.5 T are shown in Fig. 3. Here the molar core diamagnetism of $\chi_{dia}=-0.221$ memu/mol is subtracted from the data. χ_{dia} is calculated using the expression $\chi_{dia}=-0.79\times\Sigma_i Z_i\times 10^{-6}(r/a_B)^2$ emu/mol, where $\Sigma_i Z_i$ is the sum of all core electrons/f.u., (r/a_B) is roughly estimated to be unity, and a_B is the Bohr radius. In the inset of Fig. 3, a linear temperature dependence of $\chi^{-1}(T)$ is observed above 50 K. A fit according to the modified Curie-Weiss law,

$$\chi = \frac{C}{T-\Theta_{CW}} + \chi_0,$$

yields a temperature independent susceptibility $\chi_0=6.6$ memu/mol, an effective moment $\mu_{eff}=2.57\mu_B$ and the paramagnetic Curie-Weiss temperature $\Theta_{CW}=-2.6$ K. The effective magnetic moment is close to the theoretical value associated with one Ce^{3+} ion, i.e., $2.54\mu_B$, but not to the calculated value of $\mu_{eff}=3.59\mu_B$ as it is expected for the two Ce^{3+} ions in the unit cell. These data clearly indicate that in Ce_2RuZn_4 the Ce ions occur in two different valence states Ce^{3+} and Ce^{4+}. A slight curvature of the magnetic susceptibility observed below 3 K is attributed to the beginning of an antiferromagnetic transition with a Néel temperature of $T_N=2$ K as already derived from the specific-heat data.

D. Electronic structure

The investigation of the electronic structure was performed in two steps. While in a first set of calculations spin degeneracy was enforced, we considered spin polarization only at a later stage. This allowed us to investigate the influence of the magnetic order on the electronic states and the total energy in more detail.

The partial densities of states (DOSs) resulting from the first step are displayed in Figs. 4 and 5. According to Fig. 4, the densities of states are dominated by the cerium 4f states. The different behavior of the two cerium sites is clearly visible. While the 4f states of the Ce1 atoms, which are at the centers of the Zn cages, form a very sharp peak right above the Fermi energy, the linearly coordinated Ce2 4f states give rise to rather broad bands of about 1 eV width due to their overlap with the Ru 4d states.

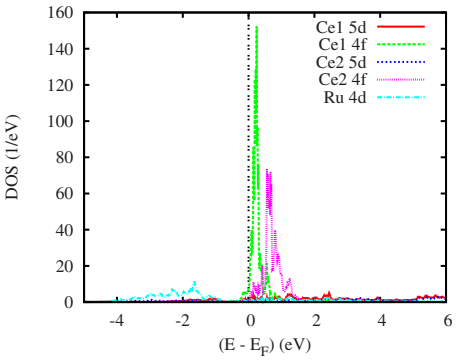

FIG. 4. (Color online) Partial densities of states of nonmagnetic Ce_2RuZn_4.

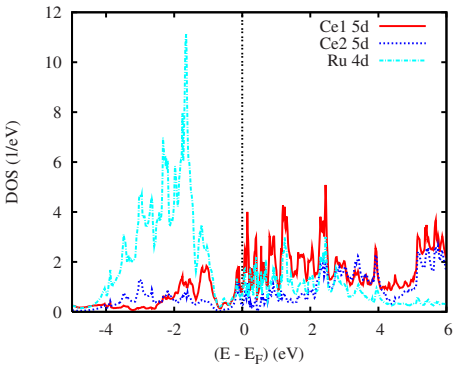

FIG. 5. (Color online) Partial densities of states of nonmagnetic Ce_2RuZn_4.

The partial DOS due to the cerium and ruthenium d states is displayed in Fig. 5. As expected, the Ru $4d$ states are located well below the Fermi energy. In contrast, the Ce $5d$ states lead to broad bands starting just slightly below E_F. Yet, hybridization of both types of bands leads to considerable contributions of the cerium and ruthenium states, respectively, below and above E_F. In particular, we observe a pronounced similarity of the Ru $4d$ partial DOS with that due to the Ce $5d$ states, which is a signature of strong d-d overlap, which is even stronger for the Ce2 sites. In passing, we mention the Zn $3d$ states, which lead to a narrow band in the energy range from −8 to −7 eV and are not included in the plot.

For simplicity reasons, subsequent spin-polarized calculations were performed for an assumed ferromagnetic order. These calculations resulted in a lowering of the total energy by about 0.9 mRy and a spin magnetic moment of about $0.4\mu_B$/f.u. Interestingly, the latter is carried by the Ce1 atoms alone, whereas the Ce2 states are not polarized. This becomes obvious from Fig. 6, which displays the partial densities of states of assumed ferromagnetic Ce_2RuZn_4. Obviously, the finite spin polarization at the Ce1 sites, which is mainly due to the $4f$ states, results from the near-E_F position of the latter. In contrast, the Ce2 $4f$ states are not polarized due to their much lower occupation.

Motivated by the strongly localized nature of the Ce $4f$ states, additional LDA+U calculations were performed with U=6.8 eV and J=0.68 eV applied at both cerium sites.

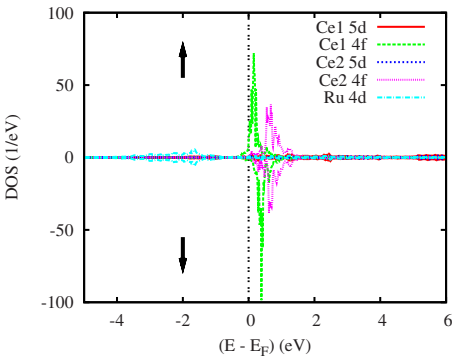

FIG. 6. (Color online) Partial densities of states of assumed ferromagnetic Ce_2RuZn_4.

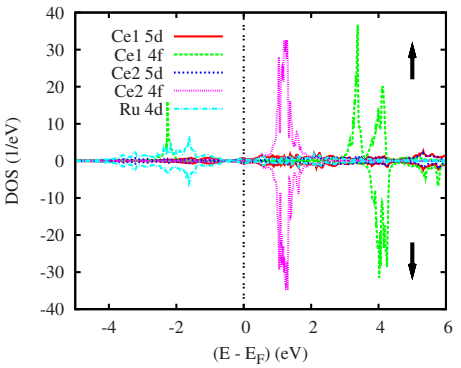

FIG. 7. (Color online) Partial densities of states of assumed ferromagnetic Ce_2RuZn_4.

These calculations resulted in a spin magnetic moment of $1.0\mu_B$ at each Ce1 site as is expected for Ce^{3+}. In contrast, the Ce2 sites remain unpolarized. In addition, a complete restructuring of the electronic states as compared to the LDA calculations is observed in the partial densities of states shown in Fig. 7. While the Ce2 $4f$ states remain centered at about 1 eV, the Ce1 $4f$ states experience a considerable splitting of about 6 eV due to the strong electronic correlations. While the spin-minority states are essentially empty, spin-majority states display a finite DOS at about −2 eV, which leads to the magnetic moments at this site. In contrast, the d states of all constituents remain essentially unpolarized except for the Ce $5d$ states, which carry small moments of $0.05\mu_B$ and $0.01\mu_B$ for Ce1 and Ce2, respectively. Since these states, like all other d states, contribute to the small but finite DOS at the Fermi energy, we interpret the polarization especially of the Ce1 $5d$ bands as being indicative of a Ruderman-Kittel-Kasuya-Yoshida (RKKY)-type exchange coupling of the localized moments.

Finally, in order to investigate the differences in chemical bonding, we display in Figs. 8 and 9 the partial covalence energies E_{cov} of assumed ferromagnetic Ce_2RuZn_4. In doing so, we concentrate on the bonding between the Ru $4d$ states with the $5d$ and the $4f$ states at the two different cerium sites. Note that negative and positive contributions to E_{cov} point to bonding and antibonding states, respectively. The E_{cov} curves are negative throughout up to E_F indicating a strong bonding between the Ru atoms and the Ce2 sites. In contrast, there is almost no bonding between the Ru atoms and the Ce1 sites, which are centered in the zinc cages.

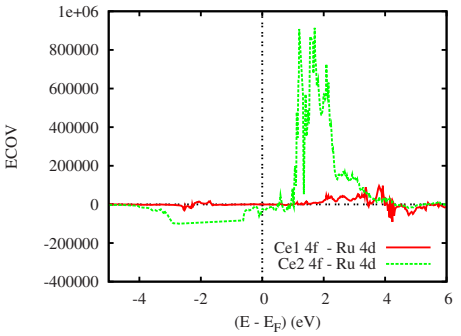

FIG. 8. (Color online) Partial covalence energies of assumed ferromagnetic Ce_2RuZn_4.

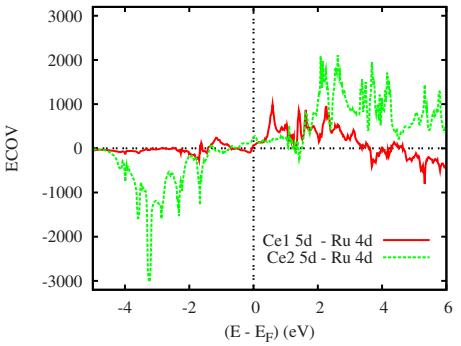

FIG. 9. (Color online) Partial covalence energies of assumed ferromagnetic Ce_2RuZn_4.

V. CONCLUSION

The intermediate-valent compound Ce_2RuZn_4 was investigated using specific-heat and susceptibility measurements as well as first-principles electronic structure calculations. This material is characterized by the presence of two different cerium sites with trivalent/intermediate valence ordering. According to the calculations, these differences go along with a striking variance in Ce-Ru bonding, which is strong at the intermediate-valent cerium sites and rather weak at the Ce1 positions at the center of the characteristic zinc cages. As a consequence, the LDA+U calculations reveal almost perfectly localized spin magnetic moments of $1.0\mu_B$ at the latter sites, whereas the Ru-bonded cerium displays no spin polarization. The theoretical findings are in full agreement with the experimental data, which point to an antiferromagnetic transition at a Néel temperature of $T_N=2$ K.

ACKNOWLEDGMENTS

This work was supported by the Deutsche Forschungsgemeinschaft through Sonderforschungsbereich 484 and Grant No. SCHE 487/7-1. W.H. is indebted to the Fonds der Chemischen Industrie for a PhD stipend.

*Corresponding author. eyert@physik.uni-augsburg.de

[1] J. Emsley, *The Elements* (Oxford University Press, Oxford, 1999).
[2] V. B. Compton and B. T. Matthias, Acta Crystallogr. **12**, 651 (1959).
[3] M. Wilhelm and B. Hillenbrand, J. Phys. Chem. Solids **31**, 559 (1970).
[4] Z. M. Kurenbaeva, A. I. Tursina, E. V. Murashova, S. N. Nesterenko, A. V. Gribanov, Y. Seropegin, and H. Noël, J. Alloys Compd. **442**, 86 (2007).
[5] E. V. Murashova, Z. M. Kurenbaeva, A. I. Tursina, H. Noël, P. Rogl, A. V. Grytsiv, A. V. Gribanov, G. Giester, and Yu. D. Seropegin, J. Alloys Compd. **442**, 89 (2007).
[6] A. I. Tursina, Z. M. Kurenbaeva, A. V. Gribanov, H. Noël, T. Roisnel, and Y. D. Seropegin, J. Alloys Compd. **442**, 100 (2007).
[7] E. V. Murashova, A. I. Tursina, Z. M. Kurenbaeva, A. V. Gribanov, and Yu. D. Seropegin, J. Alloys Compd. **454**, 206 (2008).
[8] J. F. Riecken, W. Hermes, B. Chevalier, R.-D. Hoffmann, F. M. Schappacher, and R. Pöttgen, Z. Anorg. Allg. Chem. **633**, 1094 (2007).
[9] S. F. Matar, J. F. Riecken, B. Chevalier, R. Pöttgen, A. F. Al Alam, and V. Eyert, Phys. Rev. B **76**, 174434 (2007).
[10] R. Mishra, W. Hermes, U. Ch. Rodewald, R.-D. Hoffmann, and R. Pöttgen, Z. Anorg. Allg. Chem. **634**, 470 (2008).
[11] R. Pöttgen, T. Gulden, and A. Simon, GIT Labor-Fachz. **43**, 133 (1999).
[12] D. Kußmann, R.-D. Hoffmann, and R. Pöttgen, Z. Anorg. Allg. Chem. **624**, 1727 (1998).
[13] K. Yvon, W. Jeitschko, and E. Parthé, J. Appl. Crystallogr. **10**, 73 (1977).
[14] R. Bachmann, F. J. DiSalvo, Jr., T. H. Geballe, R. L. Greene, R. E. Howard, C. N. King, H. C. Kirsch, K. N. Lee, R. E. Schwall, H. U. Thomas, and R. B. Zubeck, Rev. Sci. Instrum. **43**, 205 (1972).
[15] V. Eyert, Int. J. Quantum Chem. **77**, 1007 (2000).
[16] V. Eyert, *The Augmented Spherical Wave Method: A Comprehensive Treatment*, Lecture Notes in Physics Vol. 719 (Springer, Berlin, 2007).
[17] V. Eyert and K.-H. Höck, Phys. Rev. B **57**, 12727 (1998).
[18] V. Eyert, J. Comput. Phys. **124**, 271 (1996).
[19] P. E. Blöchl, O. Jepsen, and O. K. Andersen, Phys. Rev. B **49**, 16223 (1994).
[20] V. Eyert (unpublished).
[21] M. S. Methfessel, Phys. Rev. B **38**, 1537 (1988).